The Role of Dimethylammonium Iodide in CsPbI₃ Perovskite Fabrication: Additive or Dopant?

*Yong Wang, Xiaomin Liu, Taiyang Zhang, Xingtao Wang, Miao Kan, Jielin Shi, and Yixin Zhao**

Abstract: *The controllable growth of CsPbI₃ perovskite thin films with desired crystal phase and morphology is crucial for the development of high efficiency inorganic perovskite solar cells (PSCs). The role of dimethylammonium iodide (DMAI) used in CsPbI₃ perovskite fabrication was carefully investigated. We demonstrated that the DMAI is an effective volatile additive to manipulate the crystallization process of CsPbI₃ inorganic perovskite films with different crystal phases and morphologies. The thermogravimetric analysis results indicated that the sublimation of DMAI is sensitive to moisture, and a proper atmosphere is helpful for the DMAI removal. The time-of-flight secondary ion mass spectrometry and nuclear magnetic resonance results confirmed that the DMAI additive would not alloy into the crystal lattice of CsPbI₃ perovskite. Moreover, the DMAI residues in CsPbI₃ perovskite can deteriorate the photovoltaic performance and stability. Finally, the PSCs based on phenyltrimethylammonium chloride passivated CsPbI₃ inorganic perovskite achieved a record champion efficiency up to 19.03 %.*

Introduction

The lead halide perovskites, especially organic-inorganic hybrid perovskites, have demonstrated their unprecedented high efficiency in photovoltaic applications and various optoelectronic applications.[1–7] Recently, the CsPbI₃ inorganic perovskite without any volatile organic components has attracted much attention because of its superior chemical stability and suitable band gap among inorganic perovskites.[8–12] However, the power-conversion efficiencies (PCEs) of CsPbI₃ based perovskite solar cells (PSCs) are substantially lower than those of the organic-inorganic hybrid lead halide PSCs. The main challenge is to fabricate high quality CsPbI₃ inorganic perovskite thin film, to which different strategies have been developed.[13–19] Among them, the HI additive method was firstly reported by Snaith and co-

workers to obtain uniform black phase CsPbI₃ perovskite thin films with fine grains.[13] Consequently, the precursor of "HPbI₃" and "HPbIₓ" have been developed to improve the deposition of black phase CsPbI₃ perovskite.[14,20–25] Recently, some studies have revealed that the acid would react with the dimethylformamide (DMF) to form formic acid and dimethylamine ($(CH_3)_2NH$: DMA).[26,27] Therefore, the HI additive would induce the formation of DMAI, the previously reported "HI" additive and "HPbI₃" should be DMAI and DMAPbI₃. Hence, the role of DMAI in the fabrication of CsPbI₃ should be clarified.

In the present work, we demonstrated the fabrication of CsPbI₃ perovskite thin films by introducing different contents of DMAI additive into CsI + PbI₂ precursor. The content of DMAI additive has a significant effect on the crystal phases of CsPbI₃ perovskite and morphologies, which affect the photovoltaic (PV) performance of the corresponding PSCs devices. The sublimation of DMAI during the CsPbI₃ perovskite deposition process were explored by thermogravimetric analysis (TGA), time-of-flight secondary ion mass spectrometry (TOF-SIMS), and nuclear magnetic resonance (NMR). These results confirmed that the DMAI should be a volatile additive to control the crystallization of CsPbI₃ perovskite. No DMA dopant was found in the final CsPbI₃ perovskites after proper annealing treatment. Furthermore, we found that the DMAI residues in CsPbI₃ perovskite would deteriorate the devices PV performance and stability. With optimal DMAI additive content and phenyltrimethylammonium chloride (PTACl) passivation, we finally obtained a PTACl-CsPbI₃ based inorganic PSCs exhibiting a record champion efficiency of 19.03 %.

Results and Discussion

We firstly fabricated CsPbI₃ perovskite by simply spin coating the precursors of $CsI + PbI_2 + x\,DMAI$ ($x = 0.5$, 0.7, 1.0, 1.5), the corresponding final CsPbI₃ thin films were then denoted as Cs-*x*DMAI. Figure 1 and S1,S2 (Supporting Information) revealed that the DMAI content has a significant effect on the crystallization kinetics of perovskite, the crystal phases, and the morphologies. The crystallization process is very fast when the DMAI contents *x* are 0.5 and 0.7, as shown in Figure S1 and S2 (Supporting Information). These perovskite thin films turned into brown during the spin-coating process, a signal of the black phase perovskite formation. Figure 1a indicated that both Cs-0.5DMAI and Cs-0.7DMAI thin films have an absorbance edge at about

[*] Dr. Y. Wang, X. Liu, Dr. T. Zhang, X. Wang, M. Kan, J. Shi, Prof. Y. Zhao
School of Environmental Science and Engineering, Frontiers Science Center for Transformative Molecules, Shanghai Jiao Tong University
Shanghai 200240 (China)
E-mail: yixin.zhao@sjtu.edu.cn

Prof. Y. Zhao
Shanghai Institute of Pollution Control and Ecological Security
Shanghai 200240 (China)

Supporting information and the ORCID identification number(s) for the author(s) of this article can be found under:
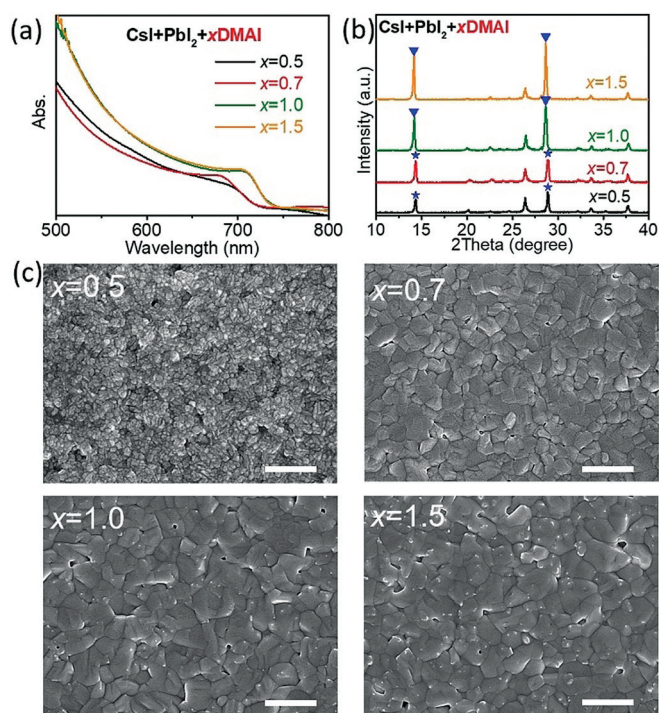https://doi.org/10.1002/anie.201910800.

Figure 1. a) UV/Vis spectra. b) XRD patterns, the star and triangle represent the characteristic peaks of γ-CsPbI₃ and β-CsPbI₃, respectively. c) SEM images of Cs-xDMAI thin films, scale bars represent 1 μm.

717 nm, which is characteristic for γ phase CsPbI₃.[11,28] The XRD patterns of the Cs-0.5DMAI and Cs-0.7DMAI thin films showed diffraction peaks at 14.3° and 28.9° (Figure 1 b and S3 in the Supporting Information), which are the characteristic (110), (220) peaks of γ-CsPbI₃ perovskite.[11,29] When x = 1.0 and 1.5, the Cs-xDMAI precursor films are light yellow during the entire spin-coating process. After annealing, the absorbance edges of both Cs-1.0DMAI and Cs-1.5DMAI thin films arise at about 736 nm (ca. 1.68 eV), which could be assigned to β-CsPbI₃ perovskite. The XRD patterns of Cs-1.0DMAI and Cs-1.5DMAI samples also exhibited the diffraction peaks at 14.2° and 28.6°, which is a typical diffraction of β-CsPbI₃ perovskite.[10,29] These results suggested that the DMAI content can significantly affect the crystal phase of the final CsPbI₃ perovskite. The scanning electron microscopy (SEM) was used to explore the morphologies of these different CsPbI₃ thin films. The DMAI content induced different crystallization processes, which lead to the different grain sizes and morphologies of Cs-xDMAI thin films. The Cs-0.5DMAI thin film exhibits compact thin film with small grain (ca. 100 nm); the crystal grain size of the Cs-0.7DMAI thin film markedly increases to circa 200–400 nm. Both the Cs-1.0DMAI and Cs-1.5DMAI thin films show similar compact morphology with larger grain size.

The above results confirmed that the DMAI additive can effectively manipulate the crystal phases and morphologies of final CsPbI₃ perovskite thin films. We carried out TOF-SIMS for the Cs-1.5DMAI sample to examine the component in the final perovskite thin films. Figure S4 in the Supporting Information showed a homogenous distribution of Cs and Pb elements. However, there are no carbon signals related to

the DMAI found in the final Cs-1.5 DMAI thin films (Supporting Information, Figure S4), which suggests the DMAI seems to be a volatile additive. In order to confirm the release of volatile DMAI additive, we used the TGA to investigate the sublimation of DMAI in the Cs-1.5DMAI samples with highest DMAI content (Figure 2 a and S5 in the
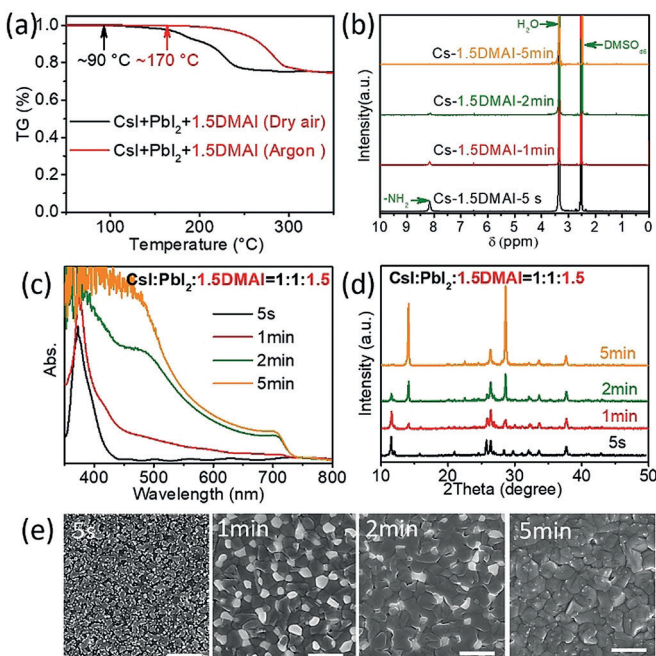

Figure 2. a) TGA of the powder scratched from the precursor film of CsI + PbI₂ + 1.5DMAI under the argon and 5–10% RH dry air conditions, respectively. b) 1H NMR of different annealing stages Cs-1.5DMAI thin films, which were dissolved in [D₆]DMSO. c) UV/Vis spectrum. d) XRD patterns, and e) SEM images of Cs-1.5DMAI thin films at different annealing stages. Scale bars represent 1 μm.

Supporting Information). Figure 2 a suggested that the DMAI can sublimate at about 170 °C from the CsI + PbI₂ + 1.5DMAI precursor powder in argon atmosphere, in which the powder is scratched from the as-deposited precursor film. Since our experiments were carried out in a dry box with 5–10% relative humidity (RH) and 20 ± 5 °C, we further investigated the TGA curve of the CsI + PbI₂ + 1.5DMAI precursor powder using the same dry air with 5–10% RH. Surprisingly, the DMAI starts to sublimate just at around 90 °C (Figure 2 a), which suggests that the moisture can significantly affect the release of DMAI additive. We further investigated the sublimation of pure DMAI powders and DMAPbI₃ (Supporting Information, Figure S5) in argon and dry air conditions, which also exhibit strong dependency on moisture. These results have strongly indicated that the DMAI is a volatile additive similar to the widely used additive MACl.[30]

Although the TGA results have indicated that the DMAI is a volatile additive, we still used NMR to confirm whether the DMAI remains in final perovskite thin films. We choose Cs-1.5DMAI sample as model sample because it has the most DMAI content in the precursor. The 1H NMR spectra of the

different annealing stages of Cs-1.5DMAI perovskite thin films in Figure 2b show a strong NMR peak related to the $-NH_2^+$-of DMA ($\delta = 8.17$ ppm) in the as-spun perovskite film with 5 s annealing. With annealing, the DMA signal decreases and totally disappears in the final 5 min annealed Cs-1.5DMAI samples. Both NMR and TOF-SIMS confirm the absence of DMAI residue in final CsPbI$_3$ perovskite, we could completely exclude the possibility of DMA dopant in final CsPbI$_3$ perovskite thin films.

All these results confirmed that the DMAI should be an additive to manipulate the CsPbI$_3$ inorganic perovskite crystallization. We further investigated the crystallization process of DMAI additive on the growth of CsPbI$_3$ inorganic perovskite. Figure 2c shows the UV/Vis spectrum evolution of the Cs-1.5DMAI precursor film during 210 °C annealing process. Initially, the absorption peak at circa 420 nm is assigned to DMAPbI$_3$ (Supporting Information, Figure S6). The absorption intensity of this peak decreases and a new absorbance with edge at 736 nm arises with the annealing progress. The crystal phase evolution during annealing process is listed in Figure 2d. The 11.6 and 12.0 degree peaks affiliated to DMAPbI$_3$ and possible intermediate phase show up in the precursor film, then slowly decrease and completely disappear in the final thin film. Simultaneously, the strong diffraction peaks at 14.2° and 28.6° gradually arise, which are assigned to (110), (220) peak of β-CsPbI$_3$.[10] The SEM images in Figure 2e list the morphology evolution of the Cs-1.5DMAI sample during annealing process. There are many small white fuzzy grains on the initial film, which could be related to the DMAPbI$_3$. With annealing, the Cs-1.5DMAI thin film shows the appearance of a dark one and the disappearance of the white grain. After 3 min annealing, all the white grains disappear, and the thin films turn into a typical black crystal grain ranging from 600 to 1000 nm (Figure 2e and S7 in the Supporting Information). These results indicated that the fresh precursor film contains the DMAI composition, and these DMAI would completely sublimate after proper annealing in 5–10% RH dry air atmosphere. Therefore, we could conclude that the DMAI only acts as a volatile additive for the controllable growth of CsPbI$_3$ inorganic perovskite.

Since all the Cs-xDMAI perovskite precursor films exhibited the characteristic absorbance and XRD pattern of DMAPbI$_3$ perovskite (Supporting Information, Figure S2). Herein, we investigated the binding energy evolution in the case of Cs-1.0DMAI sample by X-ray photoelectron spectroscopy (XPS). Figure 3a revealed that the Pb 4f7/2 at 138.3 eV in the fresh Cs-1.0DMAI precursor film could be ascribed to the Pb–I binding energy of DMAPbI$_3$ perovskite. After 5 min annealing, the peak of Pb 4f7/2 was shifted to 137.7 eV, which matches with the binding energy of Pb–I in CsPbI$_3$ perovskite. Similar binding energy shifts related to DMAPbI$_3$ to CsPbI$_3$ phase transfer were observed in I 3d and Cs 3d (Supporting Information, Figure S8). All these XPS evolution results combined with UV/Vis and XRD evolution (Supporting Information, Figure S9) indicated a possible ion exchange reaction between Cs and DMA cations during the formation of CsPbI$_3$ perovskite. It is to be noted that a strong N 1s peak at 402.2 eV from the DMA$^+$ was observed in initial

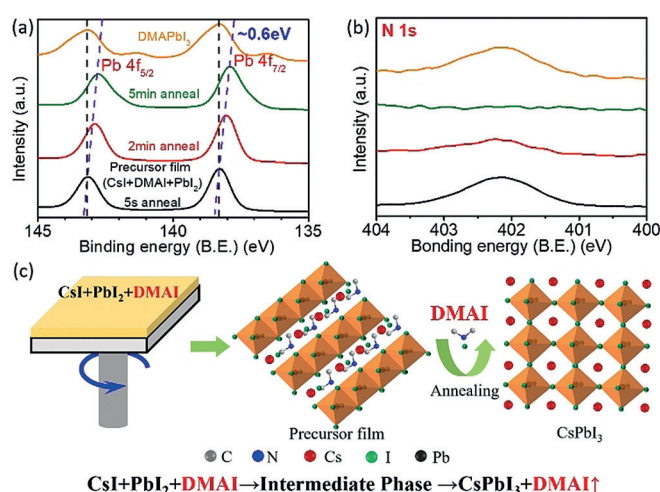**CsI+PbI$_2$+DMAI→Intermediate Phase →CsPbI$_3$+DMAI↑**

Figure 3. XPS of a) Pb 4f and b) N 1s core-level spectra for the Cs-1.0DMAI thin films at different annealing stages. c) Schematic mechanism for DMAI additive induced black phase CsPbI$_3$ formation.

stage. However, there were no signals for N 1s peak in the final thin films, which further proved the chemical nature of the CsPbI$_3$ inorganic perovskite.

All abovementioned results confirmed that the DMAI is a volatile additive in the fabrication of CsPbI$_3$ inorganic perovskite. We proposed the following growth mechanism: DMAI and PbI$_2$ would first form an intermediate phase similar to DMAPbI$_3$ perovskite, the exact structure is dependent on the DMAI content. During the annealing process, the DMAI would sublimate and the Cs$^+$ cations then enter the crystal lattice position. In the different case of Cs-xDMAI precursors, the different DMAI additive contents could affect the crystallization kinetics. When the DMAI content $x = 0.5$, 0.7, the DMAI would sublimate quickly and lead to a fast crystallization of γ-CsPbI$_3$ phase. When the x increases to 1.0 and 1.5, the slower DMAI sublimation process leads to a slower crystallization, which is beneficial for small strain in crystal lattice and the formation of slight distortion β-CsPbI$_3$ phase.

We fabricated the Cs-xDMAI perovskite thin films-based PSCs with the configuration of FTO/c-TiO$_2$/perovskite/spiro-OMeTAD/Ag. Figure 4a lists the PV parameters of Cs-xDMAI based PSCs. Figure 4b compared the typical *J–V* curves of PSCs based on Cs-xDMAI thin films under simulated AM 1.5G solar illumination of 100 mW cm^{-2} in reverse scan. The increased DMAI additive resulted in an improved PV performance. Both the Cs-0.5DMAI and Cs-0.7DMAI based PSCs devices exhibited poor PV performance. While the Cs-1.0DMAI and Cs-1.5DMAI based PSCs showed high PV performance J_{sc} (20.15 mA cm^{-2} Vs. 20.09 mA cm^{-2}), V_{oc} (1.071 V Vs. 1.066 V), FF (0.767 Vs. 0.776), PCE (16.55% Vs. 16.62%). Furthermore, the PSCs based on the CsPbI$_3$ fabricated by the high contents of DMAI additives also have small hysteresis (Supporting Information, Figure S10 and Table S1), which can be attributed to the different crystal phase, improved crystallinity and enlarged crystal grain size. The external quantum efficiency (EQE)
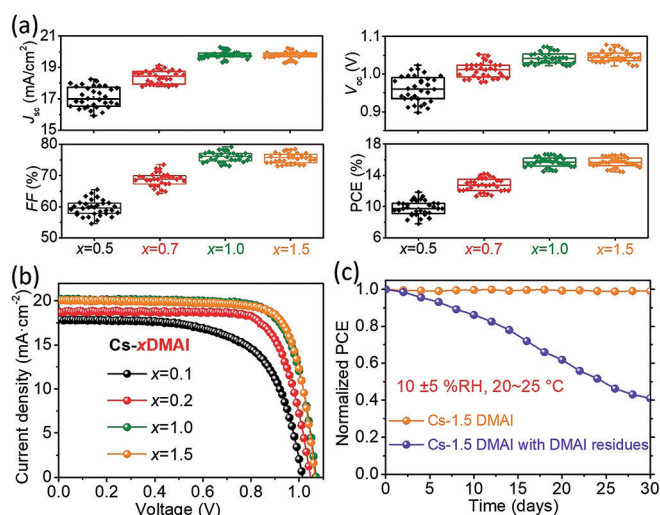
Figure 4. a) PV parameters statistics of PSCs based on Cs-xDMAI with 0.1 cm² effective cell area (32 devices). b) Corresponding champion devices J–V characteristics under simulated AM 1.5G solar illumination of 100 mW cm⁻² in reverse scan. c) Normalized PCE of the PSCs based on Cs-1.5DMAI perovskite thin films with and without DMAI residues as a function of storage time in a dark dry box under $10 \pm 5\%$ RH and 20–25 °C.

curves of these PSCs match with their *J–V* characteristics and UV/Vis spectra (Supporting Information, Figure S11).

Some previous studies suggested that DMAI containing precursor fabricated CsPbI₃ based perovskite films with DMAI residue achieved lower performance and stability.[27] Herein, we investigated the effect of DMAI residue on the final PV performance and stabilities of CsPbI₃ perovskite. We prepared the Cs-1.5DMAI sample with DMAI residue by annealing it in argon for 4 min with some DMAI residue. Unfortunately, the PSCs based on CsPbI₃ thin films with DMAI residue only achieved a PCE of 11.32% with $J_{sc} = 20.11$ mA cm⁻², $V_{oc} = 0.916$ V, and $FF = 0.615$ (Supporting Information, Figure S12). Moreover, the DMAI residues also deteriorated the stability of the device and the PSC device based CsPbI₃ layer with DMAI residue drops to about 40% of initial PCE when stored in dry air (Figure 4c). While the DMAI-residue-free CsPbI₃ PSCs based on Cs-1.5DMAI thin films show no decay after one-month storage in dry air.

The Cs-1.5DMAI based champion device has only achieved about 16.6% PCE because of the low V_{oc} and FF stemming from the defects in the perovskite layer. We then passivated the Cs-1.5 DMAI sample by spin coating 5 mM PTACl isopropanol solution, the final perovskite sample is then denoted as PTACl-CsPbI₃. Similar to previously reported PEA⁺ cations,[14,23] the organic cation PTA with hydrophobic benzene group can not only improve the humidity stability but also effectively passivate the surface defects. The absorbance of PTACl-CsPbI₃ exhibited circa 4 nm blue shift compared to that of CsPbI₃, which could be due to Cl doping in the PTACl-CsPbI₃ thin film. The morphology of PTACl-CsPbI₃ is similar to that of Cs-1.5DMAI (Supporting Information, Figure S13). The cross-section TOF-SIMS measurement revealed that the Cs and Pb are homogenously distributed (Supporting Information, Figure S14), while the

Cl dopant are mainly distributed on the top of CsPbI₃ perovskite thin films (Figure 5b). The XPS results in Figure S15 in the Supporting Information confirmed that the Cl is doped into CsPbI₃ rather than the formation of PbCl₂ or
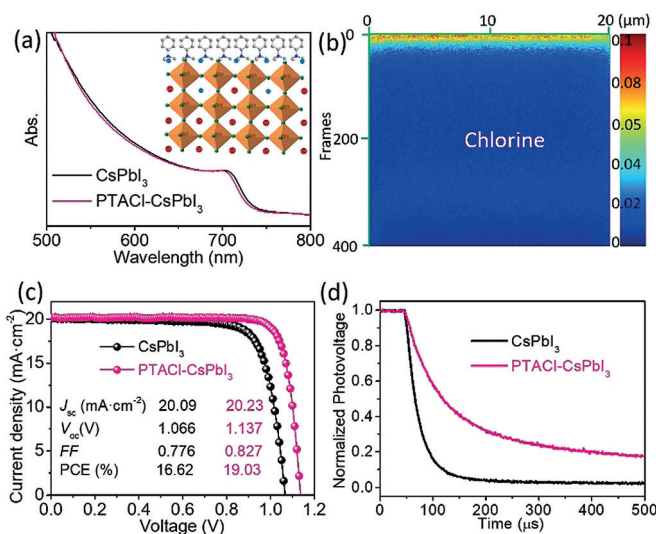

Figure 5. a) UV/Vis spectra of CsPbI₃ and PTACl-CsPbI₃ thin films. b) Cross-sectional of chlorine elemental profile of PTACl-CsPbI₃ measured by TOF-SIMS, c) J–V characteristics of PSCs based on CsPbI₃ and PTACl-CsPbI₃ under simulated AM 1.5G solar illumination of 100 mW cm⁻² in reverse scan. d) TPV of CsPbI₃ and PTACl-CsPbI₃ based PSCs.

CsCl. The XPS spectrum of the PTACl-CsPbI₃ sample exhibits the characteristic C and N signals related to the organic cation of PTACl. These PTA⁺ cations should surface terminate on CsPbI₃ rather than dope into crystal lattice because the previous study has confirmed that even the small size FA or alkyl ammonium cation would not alloy with CsPbI₃ quantum dots during the FAI or alkyl ammonium salt treatment.[12,23,31] We also investigated the impact of PTACl-treatment on the excitonic quality of perovskite films by using time-resolved photoluminescence (TRPL) spectroscopy (Supporting Information, Figure S16). The lifetime of the charge carrier ($\tau_{av} = 16.5$ ns) of PTACl-CsPbI₃ films is longer than that of the CsPbI₃ perovskite thin films ($\tau_{av} = 2.9$ ns), indicating the excellent passivation effect of Cl doping and surface terminated PTA cation.

The PTACl-CsPbI₃ based PSCs displayed a champion efficiency up to 19.03% with a J_{sc} of 20.23 mA cm⁻², V_{oc} of 1.137 V, and FF of 0.827 under reverse scan condition (Figure 5c). The PV metrics (Supporting Information, Figure S17 and Table S2) showed an average efficiency as high as 17.82%. These devices also showed small hysteresis and stabilized PCE (Supporting Information, Figure S18,19). The charge-transport properties of the PTACl-treatment PSCs were investigated by the transient photocurrent decay (TPC) and photovoltage decay (TPV) measurements. The similar TPC responses (Supporting Information, Figure S20) suggested that the PTACl treatment had minimal influence on the charge transport or charge collection efficiency, in agreement with J_{sc} and EQE results (Supporting Information,

Figure S11 and S21). In contrast, the TPV revealed that the PTACl-treatment increased charge-carrier lifetime (Figure 5 d) indicating a decrease in the undesired charge-carrier recombination.[32–35] This further proved that the strong Cl–Pb bonding together with surface terminated PTA cation can significantly passivate the surface defects. Moreover, the PTACl-CsPbI$_3$ based PSCs also exhibited good photo-stability and retained 90 % of their initial PCE after 500 h continuous illumination (Supporting Information, Figure S22).

Conclusion

We investigated the function of DMAI additive in fabricating high quality CsPbI$_3$ inorganic perovskite thin films. The DMAI additive can control the final crystal phase, crystallinity, and grain size of CsPbI$_3$ perovskite. With proper annealing process, the DMAI can be completely removed, and no DMA alloying is found in the final CsPbI$_3$ thin films. All these results demonstrated that the role of DMAI in CsPbI$_3$ fabrication should be a crystal growth additive rather than organic cation dopant. Moreover, the DMAI residues in CsPbI$_3$ perovskite would deteriorate both the PV performance and stability. An optimal DMAI additive fabricated CsPbI$_3$ perovskite with a PTACl passivation treatment can be fabricated into a champion PSC device exhibiting a record efficiency beyond 19 % with high stability.

Conflict of interest

The authors declare no conflict of interest.

Keywords: additive · all-inorganic perovskite · Cl doping · CsPbI$_3$ · dimethylammonium iodide

[1] A. Kojima, K. Teshima, Y. Shirai, T. Miyasaka, *J. Am. Chem. Soc.* **2009**, *131*, 6050–6051.

[2] H. S. Kim, C. R. Lee, J. H. Im, K. B. Lee, T. Moehl, A. Marchioro, S. J. Moon, R. Humphry-Baker, J. H. Yum, J. E. Moser, M. Gratzel, N. G. Park, *Sci. Rep.* **2012**, *2*, 591.

[3] M. M. Lee, J. Teuscher, T. Miyasaka, T. N. Murakami, H. J. Snaith, *Science* **2012**, *338*, 643–647.

[4] N. Arora, M. I. Dar, A. Hinderhofer, N. Pellet, F. Schreiber, S. M. Zakeeruddin, M. Grätzel, *Science* **2017**, *358*, 768–771.

[5] Q. Jiang, Y. Zhao, X. Zhang, X. Yang, Y. Chen, Z. Chu, Q. Ye, X. Li, Z. Yin, J. You, *Nat. Photonics* **2019**, *13*, 460–466.

[6] M. Saliba, J. P. Correa-Baena, M. Gratzel, A. Hagfeldt, A. Abate, *Angew. Chem. Int. Ed.* **2018**, *57*, 2554–2569; *Angew. Chem.* **2018**, *130*, 2582–2598.

[7] J. Gong, M. Flatken, A. Abate, J.-P. Correa-Baena, I. Mora-Seró, M. Saliba, Y. Zhou, *ACS Energy Lett.* **2019**, *4*, 861–865.

[8] A. Swarnkar, A. R. Marshall, E. M. Sanehira, B. D. Chernomordik, D. T. Moore, J. A. Christians, T. Chakrabarti, J. M. Luther, *Science* **2016**, *354*, 92–95.

[9] D. B. Straus, S. Guo, R. J. Cava, *J. Am. Chem. Soc.* **2019**, *141*, 11435–11439.

[10] Y. Wang, M. I. Dar, L. K. Ono, T. Zhang, M. Kan, Y. Li, L. Zhang, X. Wang, Y. Yang, X. Gao, Y. Qi, M. Grätzel, Y. Zhao, *Science* **2019**, *365*, 591–595.

[11] J. A. Steele, H. Jin, I. Dovgaliuk, R. F. Berger, T. Braeckevelt, H. Yuan, C. Martin, E. Solano, K. Lejaeghere, S. M. J. Rogge, C. Notebaert, W. Vandezande, K. P. F. Janssen, B. Goderis, E. Debroye, Y.-K. Wang, Y. Dong, D. Ma, M. Saidaminov, H. Tan, Z. Lu, V. Dyadkin, D. Chernyshov, V. Van Speybroeck, E. H. Sargent, J. Hofkens, M. B. J. Roeffaers, *Science* **2019**, *365*, 679–684.

[12] A. Dutta, S. K. Dutta, S. Das Adhikari, N. Pradhan, *Angew. Chem. Int. Ed.* **2018**, *57*, 9083–9087; *Angew. Chem.* **2018**, *130*, 9221–9225.

[13] G. E. Eperon, G. M. Paternò, R. J. Sutton, A. Zampetti, A. A. Haghighirad, F. Cacialli, H. J. Snaith, *J. Mater. Chem. A* **2015**, *3*, 19688–19695.

[14] T. Zhang, M. I. Dar, G. Li, F. Xu, N. Guo, M. Gratzel, Y. Zhao, *Sci. Adv.* **2017**, *3*, e1700841.

[15] C. Y. Chen, H. Y. Lin, K. M. Chiang, W. L. Tsai, Y. C. Huang, C. S. Tsao, H. W. Lin, *Adv. Mater.* **2017**, *29*, 1605290.

[16] Q. Wang, X. Zheng, Y. Deng, J. Zhao, Z. Chen, J. Huang, *Joule* **2017**, *1*, 371–382.

[17] P. Wang, X. Zhang, Y. Zhou, Q. Jiang, Q. Ye, Z. Chu, X. Li, X. Yang, Z. Yin, J. You, *Nat. Commun.* **2018**, *9*, 2225.

[18] A. Hadi, B. J. Ryan, R. D. Nelson, K. Santra, F.-Y. Lin, E. W. Cochran, M. G. Panthani, *Chem. Mater.* **2019**, *31*, 4990–4998.

[19] Z. Shao, Z. Wang, Z. Li, Y. Fan, H. Meng, R. Liu, Y. Wang, A. Hagfeldt, G. Cui, S. Pang, *Angew. Chem. Int. Ed.* **2019**, *58*, 5587–5591; *Angew. Chem.* **2019**, *131*, 5643–5647.

[20] Y. Wang, T. Zhang, M. Kan, Y. Zhao, *J. Am. Chem. Soc.* **2018**, *140*, 12345–12348.

[21] S. Xiang, Z. Fu, W. Li, Y. Wei, J. Liu, H. Liu, L. Zhu, R. Zhang, H. Chen, *ACS Energy Lett.* **2018**, *3*, 1824–1831.

[22] Y. Jiang, J. Yuan, Y. Ni, J. Yang, Y. Wang, T. Jiu, M. Yuan, J. Chen, *Joule* **2018**, *2*, 1356–1368.

[23] Y. Wang, T. Zhang, M. Kan, Y. Li, T. Wang, Y. Zhao, *Joule* **2018**, *2*, 2065–2075.

[24] J. Xi, C. Piao, J. Byeon, J. Yoon, Z. Wu, M. Choi, *Adv. Energy Mater.* **2019**, *9*, 1901787.

[25] T. Wu, Y. Wang, Z. Dai, D. Cui, T. Wang, X. Meng, E. Bi, X. Yang, L. Han, *Adv. Mater.* **2019**, *31*, 1900605.

[26] N. K. Noel, M. Congiu, A. J. Ramadan, S. Fearn, D. P. McMeekin, J. B. Patel, M. B. Johnston, B. Wenger, H. J. Snaith, *Joule* **2017**, *1*, 328–343.

[27] W. Ke, I. Spanopoulos, C. C. Stoumpos, M. G. Kanatzidis, *Nat. Commun.* **2018**, *9*, 4785.

[28] R. J. Sutton, M. R. Filip, A. A. Haghighirad, N. Sakai, B. Wenger, F. Giustino, H. J. Snaith, *ACS Energy Lett.* **2018**, *3*, 1787–1794.

[29] A. Marronnier, G. Roma, S. Boyer-Richard, L. Pedesseau, J. M. Jancu, Y. Bonnassieux, C. Katan, C. C. Stoumpos, M. G. Kanatzidis, J. Even, *ACS Nano* **2018**, *12*, 3477–3486.

[30] Y. Zhao, K. Zhu, *J. Phys. Chem. C* **2014**, *118*, 9412–9418.

[31] E. M. Sanehira, A. R. Marshall, J. A. Christians, S. P. Harvey, P. N. Ciesielski, L. M. Wheeler, P. Schulz, L. Y. Lin, M. C. Beard, J. M. Luther, *Sci. Adv.* **2017**, *3*, eaao4204.

[32] T. Leijtens, G. E. Eperon, A. J. Barker, G. Grancini, W. Zhang, J. M. Ball, A. R. S. Kandada, H. J. Snaith, A. Petrozza, *Energy Environ. Sci.* **2016**, *9*, 3472–3481.

[33] H. Tan, A. Jain, O. Voznyy, X. Lan, F. P. G. de Arquer, J. Z. Fan, R. Quintero-Bermudez, M. Yuan, B. Zhang, Y. Zhao, F. Fan, P. Li, L. N. Quan, Y. Zhao, Z.-H. Lu, Z. Yang, S. Hoogland, E. H. Sargent, *Science* **2017**, *355*, 722–726.

[34] D. Bai, J. Zhang, Z. Jin, H. Bian, K. Wang, H. Wang, L. Liang, Q. Wang, S. F. Liu, *ACS Energy Lett.* **2018**, *3*, 970–978.

[35] J. Tian, Q. Xue, X. Tang, Y. Chen, N. Li, Z. Hu, T. Shi, X. Wang, F. Huang, C. J. Brabec, H. L. Yip, Y. Cao, *Adv. Mater.* **2019**, *31*, 1901152.

16696   www.angewandte.org

© 2019 Wiley-VCH Verlag GmbH & Co. KGaA, Weinheim

Angew. Chem. Int. Ed. **2019**, *58*, 16691–16696